Atmos. Meas. Tech. Discuss., 8, 5769–5808, 2015
www.atmos-meas-tech-discuss.net/8/5769/2015/
doi:10.5194/amtd-8-5769-2015
© Author(s) 2015. CC Attribution 3.0 License.

Atmospheric Measurement Techniques Discussions
Open Access

This discussion paper is/has been under review for the journal Atmospheric Measurement Techniques (AMT). Please refer to the corresponding final paper in AMT if available.

Complex experiment on stydying the microphysical, chemical, and optical propertires of aerosol particles and estimating the contribution of atmospheric aerosol to Earth radiation budget

G. G. Matvienko[1], B. D. Belan[1], M. V. Panchenko[1], O. A. Romanovskii[1,2], S. M. Sakerin[1], D. M. Kabanov[1], S. A. Turchinovich[1], Y. S. Turchinovich[1], T. A. Eremina[1], V. S. Kozlov[1], S. A. Terpugova[1], V. V. Pol'kin[1], E. P. Yausheva[1], D. G. Chernov[1], T. B. Zhuravleva[1], T. V. Bedareva[1], S. L. Odintsov[1], V. D. Burlakov[1], A. V. Nevzorov[1], M. Yu. Arshinov[1], G. A. Ivlev[1], D. E. Savkin[1], A. V. Fofonov[1], V. A. Gladkikh[1], A. P. Kamardin[1], Yu. S. Balin[1], G. P. Kokhanenko[1], I. E. Penner[1], S. V. Samoilova[1], P. N. Antokhin[1], V. G. Arshinova[1], D. K. Davydov[1], A. V. Kozlov[1], D. A. Pestunov[1],

T. M. Rasskazchikova[1], D. V. Simonenkov[1], T. K. Sklyadneva[1], G. N. Tolmachev[1], S. B. Belan[1], V. P. Shmargunov[1], A. S. Kozlov[3], and S. B. Malyshkin[3]

[1]V. E. Zuev Institute of Atmospheric Optics SB RAS, 1 Academician Zuev sq., 634021 Tomsk, Russia
[2]National Research Tomsk State University, 36 Lenina Ave., 634050 Tomsk, Russia
[3]Voevodsky Institute of Chemical Kinetics and Combustion SB RAS, 3 Institutskaya Ave., 630090 Novosibirsk, Russia

Received: 14 April 2015 – Accepted: 18 May 2015 – Published: 12 June 2015

Correspondence to: O. A. Romanovskii (roa@iao.ru)

Published by Copernicus Publications on behalf of the European Geosciences Union.

AMTD
8, 5769–5808, 2015

Abstract

The primary objective of the Complex Aerosol Experiment was measurement of microphysical, chemical, and optical properties of aerosol particles in the surface air layer and free atmosphere. The measurement data were used to retrieve the whole set of aerosol optical parameters, necessary for radiation calculations. Three measurement cycles were performed within the Experiment during 2013: in spring, when the aerosol generation is maximal; in summer (July), when atmospheric boundary layer altitude and, hence, mixing layer altitude are maximal; and in late summer – early autumn, during the period of nucleation of secondary particles. Numerical calculations were compared with measurements of downward solar fluxes on the Earth's surface, performed in the clear-sky atmosphere in summer periods in 2010–2012 in a background region of the boreal zone of Siberia. It has been shown that, taking into account the instrumental errors and errors of atmospheric parameters, the relative differences between model and experimental values of direct and global solar radiation fluxes do not exceed, on the average, 1 and 3 %, respectively. Thus, independently obtained data on the optical, meteorological, and microphysical parameters of the atmosphere allows intercalibration and inter-complement of the data and, thereby, provide for qualitatively new information which explains the physical nature of the processes that form the vertical structure of the aerosol field.

1 Introduction

The climate change observed for already more than one decade is recognized by the whole global community. Numerous national and international programs are devoted to investigation of possible causes and prediction of further climatic tendencies. Despite the common recognition of this problem, there is no consensus on the role of human activity in the global climate change. Thus, the studies of Antarctic ice cores have shown that there were several periods of global warming for the last 650 000 years (Solomon

AMTD
8, 5769–5808, 2015

et al., 2007) accompanied by an increase in the concentration of major greenhouse gases (CO_2, CH_4, and N_2O). It was found that the increase in the temperature in the Antarctic region started several centuries before the increase in the CO_2 concentration (Monnin et al., 2001).

Although an important role of aerosols in climate changes is well established, the level of understanding of the indirect effect of aerosols in radiative changes remains very low. This fact complicates significantly the prediction of global changes in the Earth's climate.

The permanent development and improvement of climatic models requires a significantly greater amount of field measurement data from different regions of the world. The territory of Siberia occupying about 10 % of the world's land is practically not covered by the modern observation network. Meanwhile, Siberia lies in several climatic zones, its ecosystems are very different, and therefore the intensity of sources and sinks of atmospheric admixtures should vary significantly.

Taking into account the fact that every of methods for investigation of aerosol parameters is informative only in a certain wavelength range, only the combined analysis of all available experimental data can provide the correct reconstruction of the complete optical pattern of tropospheric aerosol in a particular region.

The objective of this study was simultaneous measurements of microphysical, chemical, and optical properties of aerosol particles in the surface air layer and free atmosphere with a unique set of ground-based, airborne, and spaceborne instruments in order to draw a complete pattern of the composition and state of the atmosphere over the territory of Western Siberia.

In this connection, the following tasks were formulated:

- modernization and intercalibration of developed measurement tools;
- carrying out of measurement cycles;
- retrieval of the whole set of microphysical, chemical, and optical parameters of aerosols from experimental findings;

AMTD
8, 5769–5808, 2015

– study and analysis of the influence of vertical variability of optical parameters of tropospheric aerosol on radiative effects of aerosol under typical conditions of Western Siberia.

2 Measurement system

The measurement system developed provides sun-photometric measurements of the aerosol optical depth (AOD) of the atmosphere, acoustic sounding of the boundary layer, laser sensing of the aerosol content in the troposphere and stratosphere, measurement of the gas composition of the atmosphere (including greenhouse gases), measurement of meteorological parameters of air, in particular, with weather balloons.

The composition and purpose of individual elements of the measurement system are summarized in Table 1.

Let us first consider the systems used for measurements in the surface air and then describe the devices for measuring of the integral content of the sought parameters and their vertical distributions. Continuous measurements of the concentrations of minor gas constituents (MGCs) were carried out at three IAO SB RAS stations for monitoring the atmospheric composition: Fonovaya Observatory, TOR station, and Basic Experimental Complex (BEC). The measured parameters are summarized in Table 2; the operation of all the stations is described in detail in Arshinov et al. (2007).

For controlling the measurements and the state of the systems, all data from each station are transmitted collected to the central server every hour. As a result, the state of the atmosphere is monitored in the nearly on-line mode. The graphic presentation of the monitored parameters is available on the website http://lop.iao.ru/activity/?id=mes, which is hourly updated. The interface allows selection of different options for viewing the current information both separately for each station and for a particular parameter measured at all the three stations.

AMTD
8, 5769–5808, 2015

To study the vertical distribution of the climatically significant components of the troposphere, we used the analytical equipment (Fig. 1) installed aboard the Tu-134 OPTIK flying laboratory (Anokhin et al., 2011).

Since the primary objective of the Experiment was to study radiative characteristics of the atmosphere, below we describe the equipment used to measure atmospheric admixtures being major contributors to the radiative forcing.

To study the vertical distribution of the main greenhouse gases, we used a Picarro G2301-m precision gas analyzer specially designed for in-flight measurements of carbon dioxide, methane, and water vapor concentrations with a frequency of 1 Hz (http://www.picarro.com/products_solutions/trace_gas_analyzers/co_co2_ch4_h2o). The operating principle of the gas analyzer is based on the cavity ring-down spectroscopy technique, which allows determination of the spectral characteristics of gas molecules in an optical cavity. Now this device is the world best, since the precision of CO_2, CH_4, and H_2O measurements is < 200 ppb, < 1.5 ppb, and < 150 ppm, respectively.

The ozone concentration was measured with a Thermo Environmental Instruments (TEI) Model 49C UV photometric gas analyzer modified for measurements from aircrafts of different types (Marenco et al., 1998). The measurement precision was 1 ppb at integration time of 4 s.

The vertical structure of the distribution of atmospheric aerosols was retrieved with the use of two types of devices. The first type is a diffusion aerosol spectrometer (DAS), which allows the number distribution of nanoaerosols to be retrieved in the size range from 3 to 200 nm in 20 size intervals. The DAS consists of 8-channel mesh-type diffusion battery (DB) and the condensation particle counter. The principle of particle separation by size is based on the size dependence of the diffusion coefficients of nanoparticles. As a result, particles of different sizes passing through porous media have different deposition rates: smaller particles leave the flow more quickly, and thus the coefficient of particle passage through such a medium carries the information about the particle size. The particle concentration is measured after each DB channel with a WCPC 3781 condensation particle counter (TSI inc., USA). After every scan of all

AMTD
8, 5769–5808, 2015

DB channels, the size spectrum is retrieved with the use of the algorithm developed by A. N. Ankilov and S. I. Eremenko (Eremenko and Ankilov, 1995) with regard to the WCPC 3781 counting efficiency. Due to the use of the WCPC 3781 condensation particle counter with a response time of < 2 s, the full size distribution of nanoparticles is obtained in 80 s.

The second type is a Grimm #1.109 laser aerosol spectrometer (Grimm Aerosol Technik GmbH and Co., Germany), which measures the aerosol particle number density in 31 size intervals: 0.25, 0.28, 0.3, 0.35, 0.4, 0.45, 0.5, 0.58, 0.65, 0.7, 0.8, 1.0, 1.3, 1.6, 2, 2.5, 3, 3.5, 4, 5, 6.5, 7.5, 8.5, 10, 12.5, 15, 17.5, 20, 25, 30, and 32 µm. The operating principle of this spectrometer is based on the dependence of the scattered radiation intensity on the particle size. At a known air-flow rate, the pulse repetition frequency allows the concentration of particles in air to be determined.

Thus, a combination of these two spectrometers forms an aerosol system covering the size range from 3 nm to 32 µm with a good resolution.

The temperature-wind sounding was carried out with a Vaisala DigiCORA® MW31 radiosonde (Vaisala R92SGP, http://www.vaisala.ru). The combination of this radoisonde and a GPS correlator with DigiCORA® system provides the world highest level of measurements of the atmospheric pressure (P), temperature (t), and relative air humidity (U), as well as wind measurements.

Several types of sun photometers are used in measurements of AOD and atmospheric column water vapor. In 2012, two devices were used:

1. SP-9 multiwave sun photometer for regular measurements of AOD in the 0.34–2.14 µm spectral range (16 spectral channels) and atmospheric column water vapor, as well as for retrieval of aerosol microstructure parameters (Sakerin et al., 2004, 2012);

2. CIMEL CE 318 Sun-Sky radiometer of the AERONET global network for measurements of AOD in the 0.34–1.02 µm spectral range, water vapor content W, asymmetry factor of aerosol scattering phase functions, aerosol single scattering

AMTD
8, 5769–5808, 2015

albedo, microstructure parameters of particles sized from 0.1 to 10 µm, and others (Holben et al., 1998; Dubovik et al., 1998, 2000; Dubovik and King, 2000).

Aerosol measurements at the stationary IAO SB RAS Aerosol Station (Kozlov et al., 1997, 2008a) are carried out with the use of a technique for studying aerosol properties in local air volumes, that is, air with aerosols is pumped through optical cells (flow-through measurements). The surface aerosol comes to the optical cells by ducts through air intakes installed outside the main building of IAO SB RAS at an altitude of 9 m above the surface.

The aerosol measurement system includes such devices as angle-scattering nephelometers (Kozlov et al., 2008a; Shmargunov et al., 2008), photoelectric particle counters from scattered radiation (Shmargunov and Pol'kin, 2015), and aethalometers (Kozlov et al., 1997, 2008a), that is, devices measuring characteristics of aerosol absorption. A FAN-type angular nephelometer measures the directed aerosol scattering coefficient at an angle of 45° at a wavelength of 0.51 µm, which is proportional to the concentration of submicron aerosols (Kozlov et al., 2008b). The nephelometer allows the directed scattering coefficient to be measured starting from the level of molecular scattering $\sim 1\,\mathrm{M\,m^{-1}ster^{-1}}$. The nephelometer has been calibrated under laboratory conditions against the known value of molecular scattering of radiation by pure air at the pumpdown pressure in the nephelometer cell from 760 to 350 mm Hg. To measure the disperse composition of aerosol particles, a modified PKGTA photoelectric particle counter (particle diameter of 0.4–10 µm) is used (Shmargunov and Pol'kin, 2015).

The mass concentration of black carbon in the composition of aerosol particles is measured with an MDA three-wave differential aethalometer developed at IAO SB RAS (Sakerin et al., 2004). The concentration sensitivity of the aethalometer is about $10\,\mathrm{ng\,m^{-3}}$ at 30 L of air pumped through it. The aethalometer has been calibrated under laboratory conditions with the help of a pyrolysis generator of soot (black carbon) particles and the comparison of data of synchronous optical and gravimetric measurements.

AMTD
8, 5769–5808, 2015

An aureole photometer measures the directed scattering coefficient in the angular range 1.2–20° and is used for estimation of the mass content of coarse particles in the size spectrum (Shmargunov et al., 2010).

The system of active polarization nephelometry, which is also used at the Aerosol Station, includes the FAN nephelometer and devices for artificial humidification of aerosol up to 90 % relative humidity of air or for heating up to 250 °C. It serves for the measurement of aerosol hygro- and thermograms, which are used for determination of the parameter of hygroscopic activity of particles and the fractional content of volatile compounds in aerosol. Polarization measurements with this system allow the microstructure and optical constants of submicron aerosol particles to be determined through solution of the inverse problem.

Remote laser sensing of aerosol fields in the troposphere was carried out with the stationary multifrequency LOZA lidar at three laser wavelengths of 355, 532, and 1064 nm with laser pulse repetition frequency of 20 Hz and pulse length of 10 ns. The lidar system detects not only echo signals of elastic backscattering, but also signals of Raman scattering by molecular nitrogen (387 and 607 nm) and water vapor (407 nm) at the same wavelengths in night time. Polarization components of backscattered radiation at a wavelength of 532 nm were measured in an additional channel. The multifrequency lidar provides retrieval of high-quality information about the vertical (from the surface to the lower stratosphere) distribution of optical (scattering and extinction coefficients, optical depth) and microphysical (nonsphericity, phase composition, mean size spectrum of aerosol particles within the identified layer) properties of aerosol. More detailed description of the lidar and methods for optical parameters retrieve see in Samoilova et al. (2009).

For monitoring the temperature, humidity, ozone, aerosol, and clouds with a spatial resolution of 1–10 km, the data from a MODIS multichannel spectroradiometer (spectral range 0.4–14 µm) installed on Terra and Aqua platforms of the EOS satellite system were mostly used.

AMTD
8, 5769–5808, 2015

The sounding of MGCs from space was carried out with the MetOP-A satellite IASI (Infrared Atmospheric Sounding Interferometer) Fourier spectrometer with a spectral resolution of 0.35–0.5 cm^{-1} in the range 645–2760 cm^{-1} and a spatial resolution from 25 to 100 km depending on MGC. In addition to the IASI data, the data from the Aqua AIRS (Atmospheric Infrared Sounder) with nominal spatial resolution of ~ 45 km and spectral resolution $\lambda/\Delta\lambda \sim 1200$ in 2378 channels lying in the ranges 3.74–4.61, 6.20–8.22, and 8.80–15.40 µm were used for the same purposes. The information about satellite dish can be found on http://www.orbitalsystems.com/antenna-products/systems/eosdb-systems.

The measurement system includes facilities for local and remote acoustic diagnostics of the atmospheric boundary layer, namely, METEO-2 Ultrasonic Meteostations (UMSs) (Gladkikh and Makienko, 2009) and VOLNA-4 three-channel acoustic Doppler sodar, whose main operating principles and some results are described in Gladkikh et al. (1999, 2009) and Odintsov and Fedorov (2007).

Starting from January 1996, an automated spectrophotometer installed at the Siberian Lidar Station (SLS) of IAO SB RAS carries out regular measurements of atmospheric NO_2 (nitrogen dioxide is a component of the nitrogen catalytic cycle of ozone destruction). The spectrophotometer records the spectrum of solar radiation scattered at zenith in the wavelength range 430–450 nm in twilight periods, when the solar zenith angle varies from 83 to 96°. The slant NO_2 content along the trajectory of recorded radiation is calculated from the deformation of the spectrum. The data on the slant NO_2 content in the atmosphere are used to retrieve, through solution of the inverse problem, the vertical distribution of NO_2 in 10 layers each 5 km thick in the altitude range from 0 to 50 km. Then the total NO_2 content is calculated as a sum over all the layers.

To study fluctuation parameters of the atmosphere, a multiparameter instrument has been designed. It is intended for automated measurements of wind speed pulsations, temperature, humidity, and the coefficient of angular aerosol light scattering in the surface air layer.

AMTD
8, 5769–5808, 2015

The instrument is a portable automatic device, comprising an acoustic meter of three wind velocity components and virtual temperature; an optical infrared meter of micropulsations of absolute humidity; temperature, pressure, and relative humidity sensors; and an open-type single-angle nephelometer for measuring pulsations of aerosol scattering coefficient and estimating pulsations of the atmospheric aerosol concentration. Measurements of dynamic and thermodynamic characteristics of turbulence are accompanied by measurements of solar radiation; i.e. the instrument comprises sensors of incoming and outgoing solar radiation in the visible spectral range. The temperature, humidity, wind velocity, and aerosol fields are studied to different extents; the pulsations are measured by different methods and in different periods of time. Hence, the data of these measurements are often incomparable. Therefore, the direct pulsation measurements are still urgent in the context of refinement of turbulence parameters. The instrument consists of three main spatially localized parts: modernized version of three-component ultrasonic anemometer-thermometer, spectroscopic meter of absolute humidity, and open-type nephelometer.

The developed measurement system allows one to retrieve the whole set of microphysical, chemical, and optical aerosol parameters from data measured.

3 Measuring sites

Concentrations of MGCs were routinely measured at three IAO SB RAS monitoring stations (Fig. 2): Fonovaya Observatory, TOR Station, and Basic Experimental Complex. The Fonovaya Observatory is located 70 km to the west of Tomsk, the TOR station is situated at the northeastern end of the Tomsk Scientific Center (Akademgorodok), and BEC is located in suburbs 3 km to the east from Akademgorodok (Table 3). This arrangement of the stations (nearly in line) in the case of the west–eastern air mass transport allows us to estimate the anthropogenic contribution of Tomsk to the formation of the field of atmospheric pollutants.

AMTD
8, 5769–5808, 2015

The vertical distribution of the climatically significant components of the troposphere was studied with the Tu-134 OPTIK flying laboratory.

Within the Complex Aerosol Experiment, the Tu-134 OPTIK flying laboratory carried out a sounding flight over the territory of the Ob–Tom interfluve, southwest of Tomsk (on the Kozhevnikovo–Kurlek traverse), on 9 April 2013, with the use of instruments for remote sounding and local control. The flight trajectory is shown in Figs. 3 and 4 below.

The temperature-wind sounding was carried out with the Vaisala R92SGP radiosonde.

The atmospheric AOD was monitored (in particular, on 22 May 2012) at two observation sites: in Tomsk (IAO SB RAS) and at the Fonovaya Observatory.

At the stationary Aerosol Station of IAO SB RAS located at the southeastern end of Tomsk (http://aerosol.iao.ru/?lang=en; 56.5° N, 85.1° E; GMT+7.00), surface aerosol parameters were monitored every hour round-the-clock. The Complex Aerosol Experiment on 2013 included a cycle of simultaneous two-site measurements at the IAO Aerosol Station in Tomsk and at the mobile Aerosol Station based at the Fonovaya Observatory in the forest zone 70 km to the west from Tomsk. The mass concentrations of aerosol and black carbon were measured every hour round-the-clock at the two measuring sites.

Aerosol fields of the troposphere were sensed with the LOZA-S stationary multifrequency lidar, continuously from 06:00 to 20:00 LT in 2013.

In 2013, the two-site radiative experiment was conducted in Tomsk and at the Fonovaya Observatory. This experiment invoked the data of a MODIS multichannel spectroradiometer installed on Terra and Aqua platforms of the EOS satellite system.

The acoustic diagnostics of the atmospheric boundary layer has been carried out with the use of local and remote facilities within the Complex Aerosol Experiment. Local facilities – METEO-2 USMs – were installed at the territory of the Fonovaya Observatory IAO SB RAS (Kireevsk) and in Tomsk on the roof of the laboratory building of IAO SB RAS. METEO-2 USMs operated round-the-clock in the permanent mode to measure mean values and turbulent characteristics of wind, air temperature, static

AMTD
8, 5769–5808, 2015

atmospheric pressure, and relative air humidity. The sodar operated every day from 08:00 to 21:00 LT and measured the height of the intense turbulent heat exchange layer and wind vector components in this layer (height range from 50 to 700 m).

At the IAO Siberian Lidar Station (SLS) located in Tomsk (56.5° N, 85.0° E), the automated spectrophotometer measured the nitrogen dioxide concentration in the atmosphere during morning and evening twilight.

Thus, the whole set of microphysical, chemical, and optical characteristics of aerosol in Southwestern Siberia was studied simultaneously during the Complex Aerosol Experiment (2013) with the use of the unique measurement system including ground-based, airborne, and spaceborne measurement facilities.

4 Results of complex aerosol experiment

The Experiment provided sun photometer measurements of AOD, acoustic sounding of the boundary layer, laser sensing of aerosol content in the troposphere and stratosphere, measurements of the gaseous composition of the atmosphere (including greenhouse gases), and measurements of meteorological parameters of air, including with the help of weather balloons.

The vertical aerosol and black carbon profiles were measured onboard the aircraft on 9 April (during flights near Tomsk and Zavyalovo settlement, and in the south of Novosibirsk region), 30 July (Zavyalovo settlement), and 1 October 2013 (Tomsk and Zavyalovo settlement), as shown in Fig. 5a–c, respectively.

The measurement data show that aerosol and black carbon profiles are close in shape and agree with specific features of vertical variations which we have revealed earlier. Figure 5a shows the total black carbon column up to altitudes of 7 km and aerosol mass concentration at a wavelength of 0.53 µm. These results are relatively close to springtime average values of 1.64 mg m^{-2} and 0.18, which we found earlier from results of regular aircraft measurements in the south of Western Siberia in 1999–2011 under clear sky conditions. This finding is consistent with the fact that mea-

AMTD
8, 5769–5808, 2015

surements on 9 April near Tomsk were performed under the solar weather, at a cloud amount of about 3, i.e. in the low-cloud atmosphere.

Figure 5b shows the altitude profiles of the parameters under study for the flight on 30 July 2013, in the region of Zavyalovo settlement. It is clearly seen that high aerosol and black carbon levels were observed at all altitudes in this time, primarily due to the effect of forest fire smoke plumes. The aerosol concentrations in the surface air layer were higher than 100 $\mu g\,m^{-3}$, and black carbon concentrations attained 2 $\mu g\,m^{-3}$, a factor of 3–4 higher than the mean background summertime concentrations. Thus, this flight was actually performed in the smoky atmosphere. The total black carbon column explicitly attained levels of high smoke content of the atmosphere, of about 6 $mg\,m^{-2}$, the AOD value being 1.45. Correspondingly, the smoke conditions were characterized by low particle absorption index χ (Fig. 6a) and relative black carbon content $p < 0.02$ (Fig. 6b).

Figure 5c shows the altitude profiles of the aerosol parameters under study in two regions in autumn, on 1 October 2013. Analysis of meteorological conditions during the flight showed that the preceding days were characterized by stable cloudy weather with rains and overcast cumulus clouds. The weather became better on the day of the flight, sometimes the sun was seen through the gaps; however, a few layers of diffused clouds were recorded during the flight. The presence of clouds influenced the vertical stratification of aerosol; as a consequence, the altitude profiles show the presence of two-level clouds and increased altitude variations. The total black carbon column and AOD somewhat differ from autumn average background values of 1.26 $mg\,m^{-2}$ and 0.094, respectively.

Analysis of near-ground measurements at the LAO aerosol station showed that variations in the aerosol parameters qualitatively agree with aircraft measurement results (Figs. 7–8). The analysis was performed using daily average variations in the dry bases of submicron aerosol and in black carbon normalized to their daily average values (Fig. 7). The daily variations in the condensation activity parameter γ exhibits anticor-

AMTD
8, 5769–5808, 2015

relation with the variations in the mass concentrations of submicron aerosol and black carbon (Fig. 8).

To date, the arrays of data on aerosol number density from the TOR station and Fonovaya Observatory include over 1 900 000 and 410 000 measurements, respectively. The maximal concentrations, observed at both stations, were tens of thousands of particles per cm^3. The decade average values of the total number density ranged from 1.3×10^3 to 1.2×10^4 cm^{-3} at the TOR station and from 1.4×10^3 to 5.8×10^3 cm^{-3} near the Observatory. The average aerosol number density over the entire period of observations was 4890 cm^{-3} (±4905 cm^{-3}, median = 3610 cm^{-3}) at the TOR station and 3200 cm^{-3} (±3244 cm^{-3}, median = 2561 cm^{-3}) at the Fonovaya Observatory.

The dataset accumulated allows us to classify the diurnal dynamics of aerosol number density in the atmosphere of the boreal zone of Western Siberia, and to obtain the statistics on frequency of nucleation surges. Nucleation per se cannot be recorded by present-day methods, because the detection limit of most condensation particle counters is 2–10 nm. However, considering that formation of nucleation-mode particles is associated with growth of stable clusters formed from the nucleation, surges in the nanoparticle formation henceforth will be called nucleation surges (NSs).

All days of observations were divided into three main groups: (1) nanoparticle formation event; (2) uncertain type and no in situ particle formation, i.e. when the nucleation mode was not clearly traced throughout a day; and (3) predominately bimodal total number density of particles (Aitken mode + accumulation mode).

After the particle formation events had been chosen, they were subdivided into three types. Type 1 is characterized by high concentrations of formed nucleation-mode particles ($D_p < 16$ nm) and a low concentration of coarse particles in the atmosphere. Type 1 reflects events of intense and well pronounced formation of the smallest particles, accompanied by continuous growth of the particles during 7–10 h.

Type 2 events are characterized by the behavior similar to Type 1 events, but weaker pronounced, i.e. there are single fluctuations in the size distribution, but the features of formation and further particle growth, lasting a little shorter (< 5 h) than Type 1 events,

AMTD
8, 5769–5808, 2015

are rather well discernible. Despite these differences, the formation and growth rates can be calculated for these both types at a reasonable revel of confidence.

Type 3 includes events with certain signs of new particle formation, but one of the stages is not very well discernible. These may be cases, e.g. where the process of particle formation and growth, once initiated, could then be interrupted due to effects of a number of factors, such as: cloud-caused sharp decrease in the solar radiation, air mass change (frontal passage), rain, etc. Type 3 also includes cases with weak or ill-defined particle growth.

In all, 1186 days were analyzed at the TOR station from 4 March 2010 to 30 September 2013, inclusive, and 732 days were analyzed on the territory of Fonovaya Observatory from 13 May 2011 to 30 September 2013, thus covering 91 and 83 % of the entire period of observations, respectively. Table 4 summarizes the general information on the number of days classified at both sites. Among the total number of days (TND) when the instrumentation operated normally, 283 events of nucleation surges (Type 1 + 2 + 3; 23.9 %), 705 days with no in situ aerosol formation (Type 4; 59.4 %), and 198 uncertain cases (Type 0; 16.7 %) were identified at the TOR station.

Despite the shorter data record from the Fonovaya observatory, the total frequency of surges, per cent, is comparable with the data from the TOR station: 158 (21.6 %), 508 (69.4 %), and (9.0 %), respectively. The differences are primarily explained by different numbers of days of the uncertain type. If they are excluded from the analysis (by subtracting Type 0 days from TND), the differences between the frequencies of non-occurrence of NS events (Type 4) decrease to 71.4 and 76.3 % at the TOR station and Fonovaya observatory, respectively. At the same time, the percentage of the NS events somewhat increases, to 28.6 % at the TOR station and 23.7 % in the region of Fonovaya observatory.

As an example, Fig. 9 shows some results of acoustical diagnostics of meteorological parameters of the surface air layer for each measurement cycle (10 min estimation interval):

– average air temperature T °C;

AMTD
8, 5769–5808, 2015

– vertical turbulent heat flux;

– total turbulent kinetic energy;

– vertical turbulent momentum flux (normalized to $\overline{\rho}$);

– average wind speed V_h and direction ϕ.

It should be noted that the database compiled contains a larger set of average meteorological parameters and turbulence characteristics than shown in Fig. 9. In addition, the available archive of raw experimental data permits us, if necessary, to calculate many other turbulence characteristics, which are absent in the database compiled.

The time variations in the spectral AOD, Ångström exponent α (which characterizes the selectivity of spectral dependence of AOD), and water vapor total content W of the atmosphere at two measuring sites (Tomsk and Fonovaya Observatory) are shown in Fig. 10. Comparison with average annual behavior of AOD, obtained from long-term data, shows that the springtime maximum of atmospheric turbidity did no practically appear in 2013. The main turbidity peak was observed in July–August and was caused by forest fire smokes carried from northern regions (http://fires.kosmosnimki.ru/). The selectivity exponent α ranged from 1 to 1.5, which is characteristic for a warm period. The character of variations in the water vapor total content corresponds to the average annual behavior, with low values in cold periods and increased values in summer months (with a maximum in August).

A series of experiments on laser sensing of the troposphere was performed from 2 to 11 April 2013; radiosondes were launched in some days. Figure 11 shows two examples of comparison of the aerosol spatial distribution and radiosonde data. Profiles of the backscattering coefficient in units of scattering ratio, defined as the ratio of the total to molecular scattering, are shown on a color scale. The meteorological data (temperature T, °C; pressure p, mm Hg, the vertical w and horizontal V wind velocity, $\mathrm{m\,s^{-1}}$; the relative humidity r, %; and the wind direction D, degrees) were measured with the ultrasonic meteorological station, located near the lidar at an altitude of 3 m above the

AMTD
8, 5769–5808, 2015

surface. From the radiosonde data, the relative humidity r, the wind direction D, and the equivalent-potential temperature (EPT) in degrees Kelvin are plotted.

As can be seen from Fig. 11, the meteorological situation on 3 April was characterized by the absence of clouds and considerable surface heating at negative air temperatures. The very dense surface air layer was involved in motion at 12:00 LT, the mixing layer rapidly reached a boundary layer altitude of 1 km, the aerosol density decreases, and wavelike vertical fluxes were observed. The radiosonde profiles for 08:00 LT show a decrease in the relative humidity and a wind shift above the boundary of the boundary layer. In daytime, the relative humidity also decreased above the mixing layer, and the wind shift ceased at this same boundary. In the evening, the mixing layer descended, and its boundary on the humidity profile is indiscernible.

During the project implementation in 2012–2014, we continued the lidar measurements of the optical parameters of stratospheric aerosol layer (SAL): the aerosol backscattering coefficient β_{π}^{a}, integral aerosol backscattering coefficient B_{π}^{a}, and the scattering ratio $R(H)$, defined as the ratio of the sum of aerosol and molecular backscattering coefficients to the latter. Figure 12 shows the integral aerosol backscattering coefficient measured from 1986 to 2014. The arrows show the explosive eruptions of volcanoes, after which increased aerosol content was recorded in the stratosphere over Tomsk. These data are in good agreement with data from other sites (Ridley et al., 2014).

The comparison of numerical calculation results and values of downward solar radiation fluxes on the Earth's surface measured in the clear-sky atmosphere during summer periods of 2010–2012 in a background region of boreal zone of Siberia shows that relative differences between the model and experimental values of the direct and total radiation, on the average, do not exceed 1 and 3 %, respectively, when instrumental errors and uncertainties of atmospheric parameters are considered. It is also shown that the radiative cooling rates have a local maximum of about 3.5 K day^{-1} at an altitude of about 3 km in summer. The cooling rates are much lower in winter because of a sharp increase in the water vapor total content; the $\frac{\partial T}{\partial t}$ maximum within the troposphere are

AMTD
8, 5769–5808, 2015

observed near the Earth's surface (0–0.5 km) and are caused by high absorptivity of aerosol particles in this altitude range.

The comparison of solar fluxes shows that their differences are mostly smaller or comparable with the uncertainty caused by errors in input parameters and measurements. The analysis also shows that the average differences between empirical data and model calculations are close to results obtained by other authors in other regions (Kato et al., 1997; Henzing et al., 2004; Michalsky et al., 2006; Nowak et al., 2008; Wang et al., 2009; Halthore et al., 1998, 2004; Plakhina et al., 1998; Chubarova et al., 1999). It is important that our results were obtained under the conditions of high and moderate atmospheric transmittance, where the optical depth, scattering phase function, and aerosol single scattering albedo errors increase significantly. This witnesses that models and methods used for retrieve of the optical properties of aerosol provide for generally adequate description of the aerosol radiative effects with accounting for climate conditions of Western Siberia.

5 Conclusions

The unique measurement system developed allowed simultaneous measurements of microphysical, chemical, and optical properties of aerosol particles in the surface air layer and free atmosphere with the use of different ground-based, airborne, and spaceborne facilities in order to draw a complete pattern of the composition and state of the atmosphere on the territory of Southwestern Siberia

The Complex Aerosol Experiment on measurement of different atmospheric parameters in the Siberian region in 2013 has become a first step on the way of joining the efforts of different research groups aimed at obtaining the as complete as possible information about the state of the atmosphere under conditions of changing climate. Despite the short duration of the Experiment, it has shown the potential capabilities of available measuring facilities for longer measurements in the future. In addition, the measurements have revealed some disadvantages. In particular, it was shown that the

AMTD
8, 5769–5808, 2015

capabilities of many ground-based and spaceborne instruments for active and passive sensing of the atmosphere are strongly limited by the presence of dense clouds. According to the long-term observations, only 38 cloudless days a year are observed on the average in Tomsk. In this respect, the air-borne sensing has an advantage, but the use of the flying laboratory remains limited due to the high cost. Thus, continuous combined observations seem now to be possible only in the atmospheric boundary layer.

Nevertheless, the data obtained during the Complex Aerosol Experiment are of great value both for validation, correction, and calibration of satellite measurements and for validation and improvement of climatic models.

Acknowledgements. This work was supported in part the Russian Science Foundation (Agreement no. 14-27-00022 – support for aerosol laser sensing), the Russian Foundation for Basic Research (Grants 13-05-98074, 13-05-00096, 14-05-00526, 14-05-00590), and the President of the Russian Federation (Grant NS-4714.2014.5 in support of leading scientific schools).

References

Anokhin, G. G., Antokhin, P. N., Arshinov, M.Yu., Barsuk, V. E., Belan, B. D., Belan, S. B., Davydov, D. K., Ivlev, G. A., Kozlov, A. V., Kozlov, V. S., Morozov, M. V., Panchenko, M. V., Penner, I. E., Pestunov, D. A., Sikov, G. P., Simonenkov, D. V., Sinitsyn, D. S., Tolmachev, G. N., Filipov, D. V., Fofonov, A. V., Chernov, D. G., Shamanaev, V. S., and Shmargunov, V. P.: OPTIK Tu-134 aircraft laboratory, Atmos. Ocean. Opt., 24, 805–816, 2011. 5774

Arshinov, M.Yu., Belan, B. D., Davydov, D. K., Ivlev, G. A., Kozlov, A. V., Pestunov, D. A., Pokrovskii, E. V., Tolmachev, G. N., and Fofonov, A. V.: Sites for monitoring of greenhouse gases and gases oxidizing the atmosphere, Atmos. Ocean. Opt., 20, 45–53, 2007. 5773

Chubarova, N. E., Rublev, A. N., Trotsenko, A. N., and Trembach, V. V.: Comparisons between modeled and measured surface shortwave irradiances under clear sky conditions, Izv. Atmos. Ocean. Phys., 35, 201–216, 1999. 5787

Dubovik, O. and King, M.: A flexible inversion algorithm for retrieval aerosol optical properties from Sun and sky radiance measurements, J. Geophys. Res., 105, 20673–20696, 2000. 5776

AMTD

8, 5769–5808, 2015

Dubovik, O., Holben, B., Kaufman, Y., Yamasoe, M., Smirnov, A., Tanre, D., and Slutsker, I.: Single-scattering albedo of smoke retrieved from the sky radiance and solar transmittance measured from ground, J. Geophys. Res., 103, 31903–31923, 1998. 5776

Dubovik, O., Smirnov, A., Holben, B., King, M., Kaufman, Y., Eck, T., and Slutsker, I.: Accuracy assessments of aerosol optical properties retrieved from Aerosol Robostic Network (AERONET) Sun and sky radiance measurements, J. Geophys. Res., 105, 9791–9806, 2000. 5776

Eremenko, S. and Ankilov, A.: Conversion of the diffusion battery data to particle size distribution: multiple Solutions Averaging algorithm (MSA), J. Aerosol Sci., 26, 749–750, 1995. 5775

Gladkikh, V. A. and Makienko, A. E.: Digital ultrasonic meteostation, Pribory, 109, 21–25, 2009. 5778

Gladkikh, V. A., Makienko, A. E., and Fedorov, V. A.: Volna-3 Doppler sodar, Atmos. Ocean. Opt., 12, 422–429, 1999. 5778

Gladkikh, V. A., Kamardin, A. P., and Nevzorova, I. V.: Determination of internal mixing layer height from "Volna" sodar measurements, Atmos. Ocean. Opt., 22, 1154–1159, 2009. 5778

Halthore, R. N., Nemesure, S., Schwartz, S. E., Emre, D. G., Berk, A., Dutton, E. G., and Bergin, M. H.: Models overestimate diffuse clear-sky irradiance: a case for excess atmospheric absorption, Geophys. Res. Lett., 25, 3591–3594, 1998. 5787

Halthore, R. N., Miller, M. A., Ogren, J. A., Sheridan, P. J., Slater, D. W., and Stoffel, T.: Further developments in closure experiments for diffuse irradiance under cloud-free skies at a continental site, Geophys. Res. Lett., 31, L07111, doi:10.1029/2003GL019102, 2004. 5787

Henzing, J. S., Knap, W. H., Stammes, P., Apituley, A., Bergwerff, J. B., Swart, D. P. J., Kos, G. P. A., and ten Brink, H. M.: Effect of aerosols on the downward shortwave irradiances at the surface: measurements vs. calculations with MODTRAN4.1, J. Geophys. Res., 109, D14204, doi:10.1029/2003JD004142, 2004. 5787

Holben, B. N., Eck, T. F., Slutsker, I., Tanre, D., Buis, J. P., Setzer, A., Vermote, E., Reagan, J. A., Kaufman, Y. J., Nakadjima, T., Lavenu, F., Jankowiak, I., and Smirnov, A.: AERONET – a federated instrument network and data archive for aerosol characterization, Remote Sens. Environ., 66, 1–16, 1998. 5776

Kato, S., Ackerman, T. P., Clothiaux, E. E., Mather, J. H., Mace, G. G., Wesely, M. L., Murcray, F., and Michalsky, J.: Uncertainties in modeled and measured clear-sky surface shortwave irradiances, J. Geophys. Res., 102, 25881–25898, 1997. 5787

AMTD
8, 5769–5808, 2015

Kozlov, V. S., Panchenko, M. V., Tumakov, A. G., Shmargunov, V. P., and Yausheva, E. P.: Some peculiarities of the mutual variability of the content of soot and submicron aerosol in the near-ground air layer, J. Aerosol Sci., 28, S231–S232, 1997. 5776

Kozlov, V. S., Panchenko, M. V., and Yausheva, E. P.: Mass fraction of Black Carbon in submicron aerosol as an indicator of influence of smokes from remote forest fires in Siberia, Atmos. Environ., 42, 2611–2620, doi:10.1016/j.atmosenv.2007.07.036, 2008a. 5776

Kozlov, V. S., Shmargunov, V. P., and Pol'kin, V. V.: Spectrophotometers for investigation of characteristics of radiation absorption by aerosol particles, Prib. Tekh. Eksp., 5, 155–157, 2008b. 5776

Marenco, A., Thouret, V., Nedelec, P., Smit, H., Helten, M., Kley, D., Karcher, F., Simon, P., Law, K., Pyle, J., Poschmann, G., Von Wrede, R., Hume, C., and Cook, T.: Measurement of ozone and water vapor by Airbus in-service aircraft: the MOZAIC airborne program, an overview, J. Geophys. Res.-Atmos., 103, 25631–25642, 1998. 5774

Michalsky, J. J., Anderson, G. P., Barnard, J., Delamere, J., Gueymard, C., Kato, S., Kiedron, P., McComiskey, A., and Ricchiazzi, P.: Shortwave radiative closure studies for clear skies during the Atmospheric Radiation Measurement 2003 Aerosol Intensive Observation Period, J. Geophys. Res., 111, D14S90, doi:10.1029/2005JD006341 2006. 5787

Monnin, E., Indermuhle, A., Dallenbach, A., Fluckinger, J., Stauffer, B., Stocker, T. F., Raynaud, D., and Barnola, J.-M.: Atmospheric CO_2 concentrations over the last glacial termination, Science, 291, 112–114, 2001. 5772

Nowak, D., Vuilleumier, L., Long, C. N., and Ohmura, A.: Solar irradiance computations compared with observations at the Baseline Surface Radiation Network Payerne site, J. Geophys. Res., 2008, 113, D14206, doi:10.1029/2007JD009441, 2008. 5787

Odintsov, S. L. and Fedorov, V. A.: Investigation of wind velocity variations on mesometeorological scale from sodar observations, Atmos. Ocean. Opt., 20, 900–906, 2007. 5778

Plakhina, I. N., Repina, I. A., and Gorchakova, I. A.: Comparison between measured and calculated radiation fluxes reaching the Earth's surface, Izv. Atmos. Ocean. Phys., 34, 112–119, 1998. 5787

Ridley, D. A., Solomon, S., Barnes, J. E., Burlakov, V. D., Deshler, T., Dolgii, S. I., Herber, A. B., Nagai, T., Neely III, R. R., Nevzorov, A. V., Ritter, C., Sakai, T., Santer, B. D., Sato, M., Schmidt, A., Uchino, O., and Vernier, J. P.: Total volcanic stratospheric aerosol optical depths and implications for global climate change, Geophys. Res. Lett., 41, 7763–7769, doi:10.1002/2014GL061541, 2014. 5786

AMTD
8, 5769–5808, 2015

Sakerin, S. M., Kabanov, D. M., Rostov, A. P., Turchinovich, S. A., Turchinovich, and Yu, S.: System for the network monitoring of the atmospheric constituents active in radiative processes, Part 1. Sun photometers, Atmos. Ocean. Opt., 17, 314–320, 2004. 5775, 5776

Sakerin, S. M., Kabanov, D. M., Rostov, A. P., Turchinovich, S. A., and Knyazev, V. V.: Sun photometers for measuring the spectral atmospheric transparency under stationary and mobile conditions, Atmos. Ocean. Opt., 25, 1112–1117, 2012. 5775

Samoilova, S. V., Balin, Yu. S., Kokhanenko, G. P., and Penner, I. E.: Investigation of the tropospheric aerosol layer vertical distribution from the data of sensing with a multifrequency Raman lidar, Part 1. Methods for the reconstruction of optical parameters, Atmos. Ocean. Opt., 22, 344–357, 2009. 5777

Shmargunov, V. P. and Pol'kin, V. V.: AZ-5 based aerosol counter, Prib. Tekh. Eksp., 2, 165–166, 2007. 5776

Shmargunov, V. P., Kozlov, V. S., Tumakov, A. G., Pol'kin, V. V., and Panchenko, M. V.: FAN-based automated aerosol nephelometer, Prib. Tekh. Eksp., 5, 165–167, 2008. 5776

Shmargunov, V. P., Pol'kin, V. V., Tumakov, A. G., Panchenko, M. V., and Pol'kin, V. V.: Closed-volume aureole photometer, Prib. Tekh. Eksp., 6, 155–157, 2010. 5777

Solomon, S., Qin, D., Manning, M., Chen, Z., Marquis, M., Averyt, K. B., Tignor, M., and Miller, H. L.: Climate Change 2007: The Physical Science Basis, Contribution of Working Group I to the Fourth Assessment Report of the Intergovernmental Panel on Climate Change, IPCC AR4 WG1, Cambridge University Press, 2007. 5771

Wang, P., Knap, W. H., Munneke, P. K., and Stammes, P.: Clear-sky shortwave radiative closure for the Cabauw baseline surface radiation network site, Netherlands, J. Geophys. Res., 114, D14206, doi:10.1029/2009JD011978, 2009. 5787

AMTD
8, 5769–5808, 2015

Table 1. Composition and purpose of individual elements of the measurement system.

No.	Element	Produced by	Measurements since	Purpose	URL
1	TOR station	IAO SB RAS, RUSSIA	1992	Monitoring of meteorological parameters, gas and aerosol composition of air, and solar radiation in the surface layer	http://lop.iao.ru/eng/index.php/about-tor-station/aero-tor
2	Basic Experimental Complex	IAO SB RAS, RUSSIA	1986	Monitoring of meteorological parameters, gas and aerosol composition of air, and solar radiation in the surface layer	http://lop.iao.ru/eng/index.php/about-bec/aerosols
3	Fonovaya (Background) Observatory	IAO SB RAS, RUSSIA	1978	Monitoring of meteorological parameters, gas and aerosol composition of air, and solar radiation in the surface layer	http://lop.iao.ru/eng/index.php/about-fonovyi/aerosols-2
4	Ty-134 OPTIK flying laboratory	IAO SB RAS, RUSSIA	1988	Measurement of meteorological parameters, gas and aerosol composition of air, optical characteristics of air	http://www.iao.ru/en/resources/equip/plane/
5	DigiCORA 3 system for radio sounding of the atmosphere	Vaisala Oy, Finland	2006	Determination of vertical distribution of meteorological parameters by contact tools	http://www.vaisala.fi/Vaisala_Documents/Brochures_and_Datasheets/MW31-for-MET-Datasheet-B210361EN-E-LOW.pdf
6	SP-9 sun photometer	IAO SB RAS, RUSSIA	2010	Measurement of aerosol optical depth and water column of the atmosphere	http://link.springer.com/article/10.1134/S102485601304012X
7	Aerosol Station	IAO SB RAS, RUSSIA	1996	Measurements of characteristics of surface aerosol	http://aerosol.iao.ru/?lang=en
8	LOZA Lidar	IAO SB RAS, RUSSIA	1992	Determination of aerosol profile at a distance of 1–10 km in any direction of the hemisphere	http://www.iao.ru/en/resources/equip/lidars
9	2.4 XLB Direct Broadcast Reception System	Orbital Systems, USA	2011	Reception of satellite data from AVHRR, MODIS, and other optoelectronic devices	http://www.orbitalsystems.com/antenna-products/systems/eosdb-systems/
10	METEO-2 Ultrasonic Meteostation	IAO SB RAS, RUSSIA	2007	Measurement of mean values and characteristics of wind turbulence and air temperature	http://www.iao.ru/en/resources/equip/dev/meteo2
11	VOLNA Sodar	IAO SB RAS, RUSSIA	2006	Measurement of vertical profiles of wind vector components in the atmospheric boundary layer	http://www.iao.ru/en/resources/equip/dev/sodar
12	Siberian Lidar Station	IAO SB RAS, RUSSIA	1988	High-altitude sensing of the atmosphere	http://www.iao.ru/en/resources/equip/sls/

AMTD
8, 5769–5808, 2015

Table 2. Measurement facilities and their characteristics.

TOR station					
Unit	Device/sensor	Parameter	Range	Error	Time constant
Weather station	HIH-3602-C	t, °C	−40...+85	±0.1 °C	1 s
	HIH-3602-C	U,%	0...100	±2 %	1 s
	M-63	dd, deg	0...360	±10°	1 s
	M-63	V, m s^{-1}	1.2...40	± (0.5+0.05 V)	1 s
	MPX4115AP	P, hPa	150...1150	±1.5	0.001 s
Gas analyzer	G2301-m	CO_2, ppm	0...1000	< 0.2 ppm	1 s
		CH_4, ppm	0...20	< 0.0015 ppm	1 s
		H_2O, ppm	0...70 000	< 150 ppm	1 s
	3.02-П	O_3, µg m^{-3}	0...500	±20 %	1 s
	P-310	NO/NO_2, µg m^{-3}	0...1000	±25 %	160 s
	K-100	CO, mg m^{-3}	0...50	±20 %	1 s
	API 100E	SO_2, ppm	0...20	±0.5 %	20 s
	Brewer 049	TO, DU	–	±1 %	120 s
Aerosol system	GRIMM #1.109	D_p, µm (31 channels)	0.25...32	–	6 s
		N, cm^{-3}	0...2000	±3 %	
	Diffusion aerosol spectrometer	D_p, nm (20 channels)	3...200	–	80 s
		N, cm^{-3}	0...500 000	±10 %	
Air ions	Sapfir-3M	N, cm^{-3}	0...2 500 000	±5 %	4 s
Radiation unit	M-115	λ, µm	0.3...2.4	±10 %	< 40 s
		Q, W m^{-2}	0...1500		
	YES UVB-1	λ, nm	280...320	–	0.1 s
		I, W m^{-2}	0...2.5	< 5 %	
	Brewer 049	λ, nm	290...325	–	265 s
		I, W m^{-2}	–	–	
Gamma background	IRF	γ-background, $\mu R/h$	1...1000	30 %	1 s
BEC					
Unit	Device/sensor	Parameter	Range	Error	Time constant
Weather station	HIH-3602-C	t, °C	−40... +85	±0.1 °C	1 s
	HIH-3602-C	U,%	0...100	±2 %	1 s
	M-63	dd, deg	0...360	±10°	1 s
	M-63	V, m s^{-1}	1.2...40	± (0.5+0.05 V)	1 s
	MPX4115AP	P, hPa	150...1150	±1.5	0.001 s
Gas analyzer	LI-820	CO_2, ppm	0...1000	< 0.2* ppm	1 s
	3.02-П	O_3, µg m^{-3}	0...500	±20 %	1 s
	API 200E	NO/NO_2, ppm	0...20	±0.5 %	20 s
	K-100	CO, mg m^{-3}	0...50	±20 %	1 s
	ME 9850B	SO_2, ppm	0...20	±1 %	< 20 s
	HCNM 2000G	CH_4 and ΣCH, ppm	0...10	0.1	120 s
Aerosol system	GRIMM #1.108	D_p, µm (15 channels)	0.3...20	–	6 s
		N, cm^{-3}	0...2000	±3 %	

AMTD
8, 5769–5808, 2015

Table 2. Continued.

Fonovaya Observatory					
Unit	Device/sensor	Parameter	Range	Error	Time constant
Weather station	HIH-3602-C	t, °C	−40... +85	±0.1 °C	1 s
	HIH-3602-C	U,%	0...100	±2 %	1 s
	M-63	dd, deg	0...360	±10°	1 s
	M-63	V, m s^{-1}	1.2...40	± (0.5+0.05 V)	1 s
	MPX4115AP	P, hPa	150...1150	±1.5	0.001 s
Gas analyzer	FGGA	CO_2, ppm	20...10 000	0.2 ppm	1 s
	Model 907-0010	CH_4, ppm	0.005...50	0.001 ppm	
		H_2O, ppm	150...70 000	100 ppm	
	LI-840	CO_2, ppm	0...1000	< 0.2* ppm	1 s
	3.02-P	O_3, µg m^{-3}	0...500	±20 %	1 s
	P-310	NO/NO_2, µg m^{-3}	0...1000	±25 %	160 s
	K-100	CO, mg m^{-3}	0...50	±20 %	1 s
	C-310	SO_2, mg m^{-3}	0...2	±25 %	142 s
Aerosol system	GRIMM #1.108	D_p, µm (15 channels)	0.3...20	–	6 s
		N, cm^{-3}	0...2000	±3 %	
	Diffusion aerosol spectrometer	D_p, nm (20 channels)	3...200	–	160 s
		N, cm^{-3}	0...1 000 000	±10 %	
Air ions	Sapfir-3M	N, cm^{-3}	0...2 500 000	±5 %	4 s

* at calibration against control gas mixtures.

AMTD
8, 5769–5808, 2015

Table 3. Coordinates of the stations.

Station	Latitude	Longitude	Altitude above mean sea level
TOR	56°28′41″	85°03′15″	133
Fonovaya1	56°25′07″	84°04′27″	80
BEC	56°28′49″	85°06′08″	120

AMTD
8, 5769–5808, 2015

Table 4. Total number of days when nanoparticles formed in situ (Types 1, 2, and 3), type was uncertain (Type 0), and no nucleation (Type 4)) was observed over the entire measurement period. ND means no data available, i.e. days when the instrumentation did not work for any reasons; TND means the total number of days analyzed.

Month	Type 1	Type 2	Type 3	Type 0	Type 4	ND	TND
TOR station							
1	1	1	5	11	69	6	87
2	3	2	4	10	63	3	82
3	20	20	9	23	40	12	112
4	30	11	7	21	31	20	100
5	15	19	6	28	52	4	120
6	3	6	15	18	63	13	105
7	2	10	6	22	58	26	98
8	7	12	7	24	66	8	116
9	17	11	7	18	64	3	117
10	7	6	3	13	58	6	87
11	2	2	0	5	66	15	75
12	2	2	3	5	75	6	87
Total	109	102	72	198	705	122	1186
Fonofaya Observatory							
1	0	1	4	5	46	6	56
2	4	1	7	9	36	0	57
3	7	5	5	6	25	14	48
4	10	11	9	5	20	5	55
5	3	5	8	5	31	41	52
6	2	2	6	9	53	18	72
7	1	4	3	5	60	20	73
8	3	4	6	5	66	9	84
9	17	8	6	7	39	13	77
10	5	3	0	3	44	7	55
11	1	0	6	3	43	7	53
12	0	0	1	4	45	12	50
Total	53	44	61	66	508	152	732

AMTD
8, 5769–5808, 2015

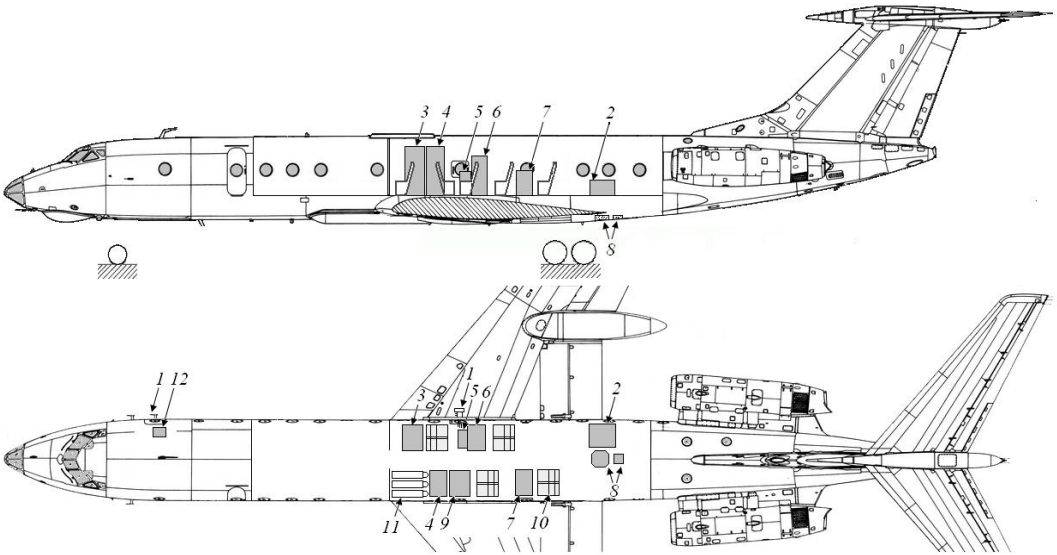

Figure 1. Arrangement of scientific equipment onboard the Tu-134 OPTIK flying laboratory: 1 – air intakes; 2 – power supply unit for airborne equipment; 3 – instrument rack for the gas analyzers: O_3 (TEI Model 49C), SO_2 (T-API 100E), and DAS (diffusion aerosol spectrometer); 4 – instrument rack for the gas analyzers: CO_2 (CONDOR), $CO_2/CH_4/H_2O$ (Picarro G2301-m), O_3 (TEI Model 49C), and CO (TEI Model 48C); 5 – rack for the filter-aspiration setup, laser aerosol spectrometer (Grimm Model 1.109), and O_3 gas analyzer (OPTEK 3.02P); 6 – instrument rack for aethalometer and flow-through nephelometer (FAN); 7 – rack for the central onboard computer; 8 – camera windows; 9 – instrument rack for the CO_2 gas analyzer (LI-6262) and portal of air sampling into flasks; 10 – operator chairs; 11 – span gas cylinders; 12 – device for sampling onto filters for analysis of the organic component of aerosol.

AMTD
8, 5769–5808, 2015

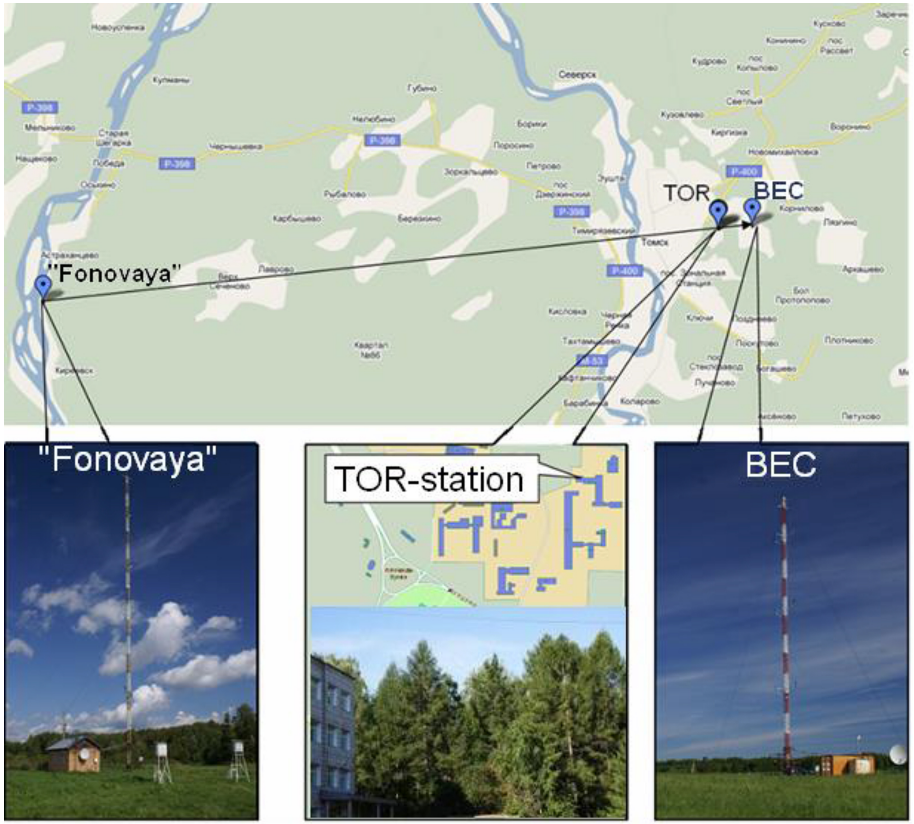

Figure 2. Arrangement of stations for atmospheric monitoring.

AMTD
8, 5769–5808, 2015

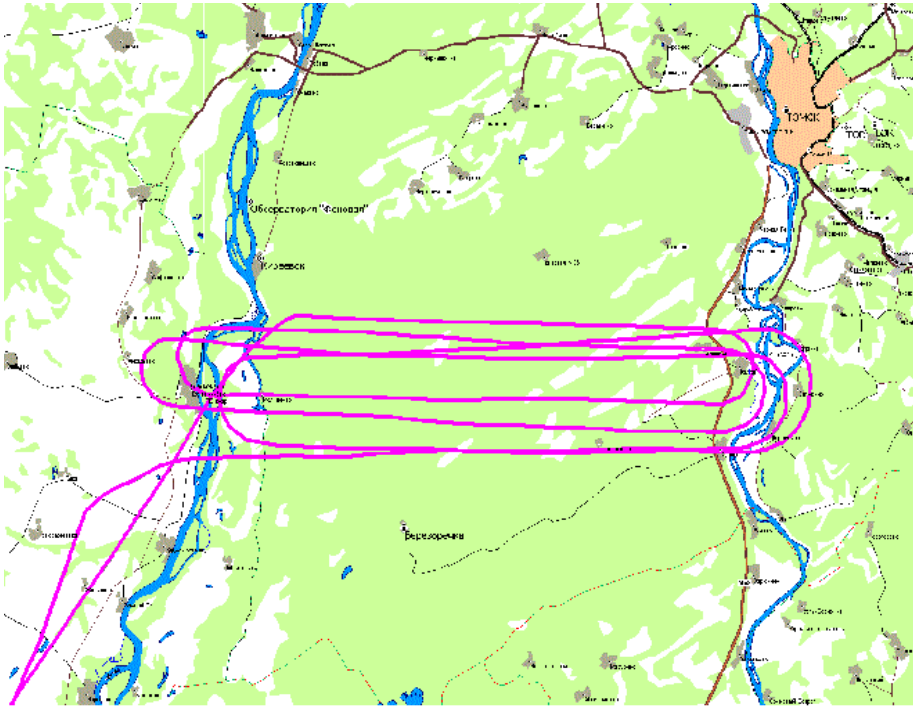

Figure 3. Flight trajectory of the Tu-134 OPTIK flying laboratory on 9 April 2013.

AMTD
8, 5769–5808, 2015

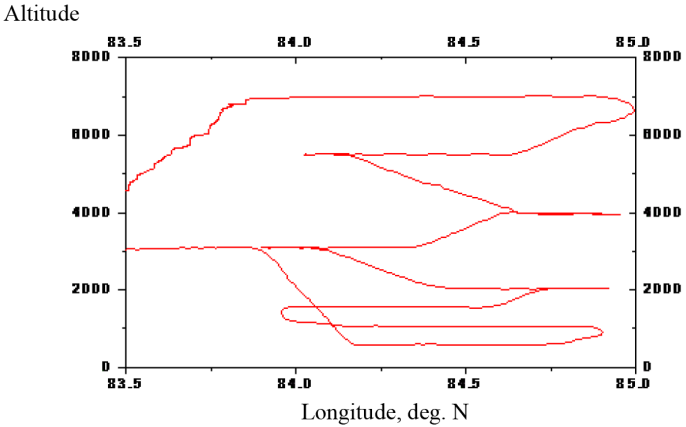

Figure 4. Altitude profile of the flight of the Tu-134 OPTIK flying laboratory on 9 April 2013.

AMTD
8, 5769–5808, 2015

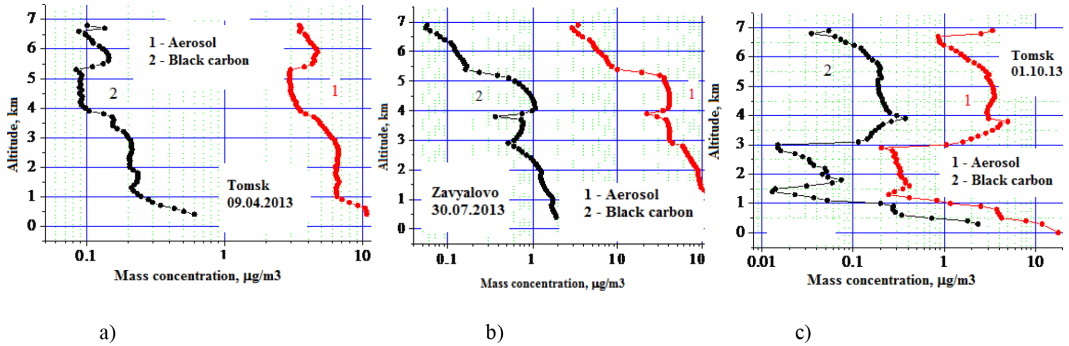

Figure 5. Vertical aerosol and black carbon profiles from flying laboratory data in the Tomsk region for **(a)** 9 April (near Tomsk and Zavyalovo settlement, south of Novosibirsk region); **(b)** 30 July (Zavyalovo settlement); and **(c)** 1 October 2013 (Tomsk and Zavyalovo settlement).

AMTD
8, 5769–5808, 2015

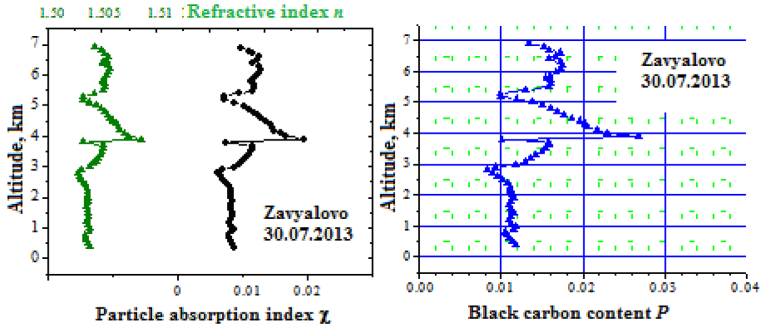

a) b)

Figure 6. Altitude profiles of **(a)** refractive and absorption indices of dry aerosol base and **(b)** relative black carbon content during the flight on 30 July 2013, in the region of Zavyalovo settlement.

AMTD
8, 5769–5808, 2015

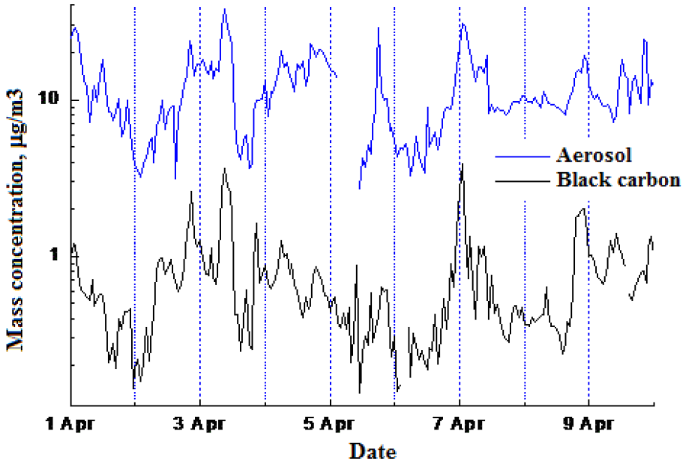

Figure 7. Time variations in the mass concentrations of dry base of submicron aerosol and black carbon during 1–9 April 2013.

AMTD
8, 5769–5808, 2015

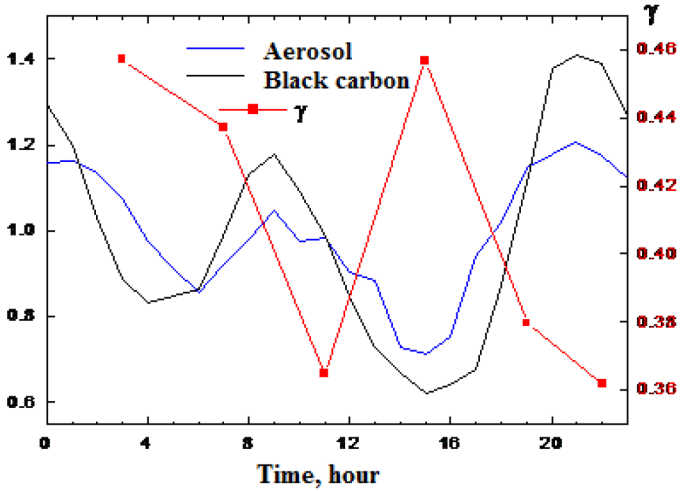

Figure 8. Normalized daily average variations in the mass concentrations of dry base of submicron aerosol and black carbon, smoothed using 3-point moving average, and daily average variations in the condensation activity parameter during 1–9 April 2013.

AMTD
8, 5769–5808, 2015

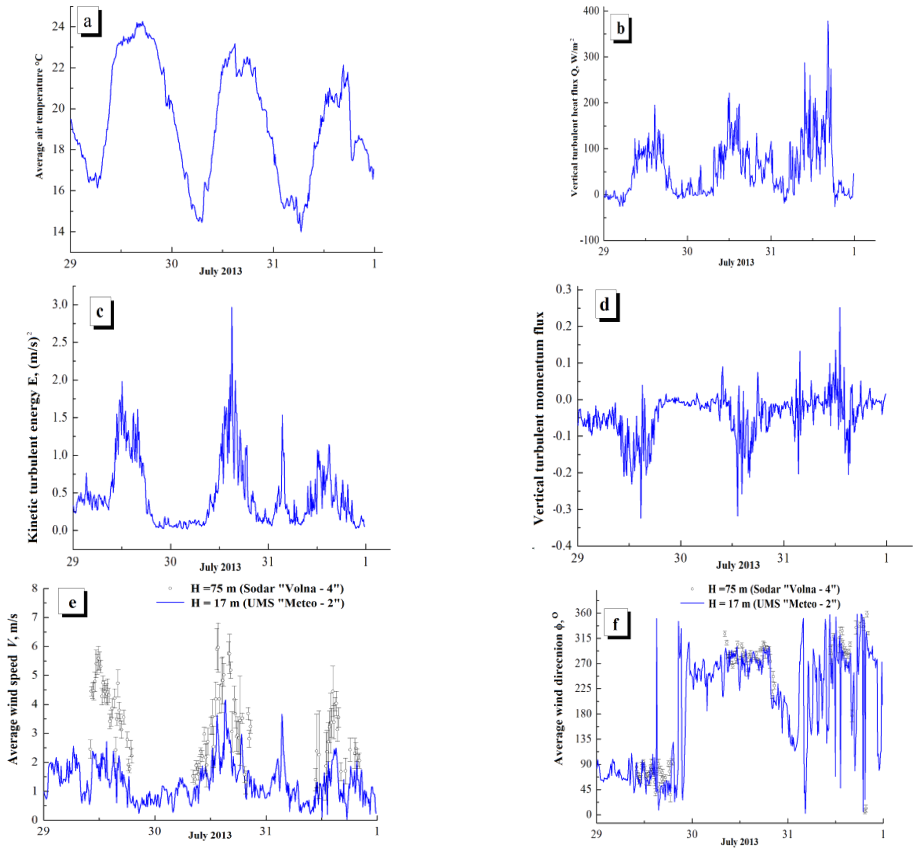

Figure 9. Time variations in the **(a)** air temperature, **(b)** vertical turbulent heat flux, **(c)** kinetic turbulent energy, **(d)** vertical turbulent momentum flux, and wind **(e)** speed and **(f)** direction at an altitude of 17 m during the first cycle of measurements. The circles (**e** and **f**) show the wind speed and direction (with 90 % confidence intervals) at an altitude of 50 m.

AMTD
8, 5769–5808, 2015

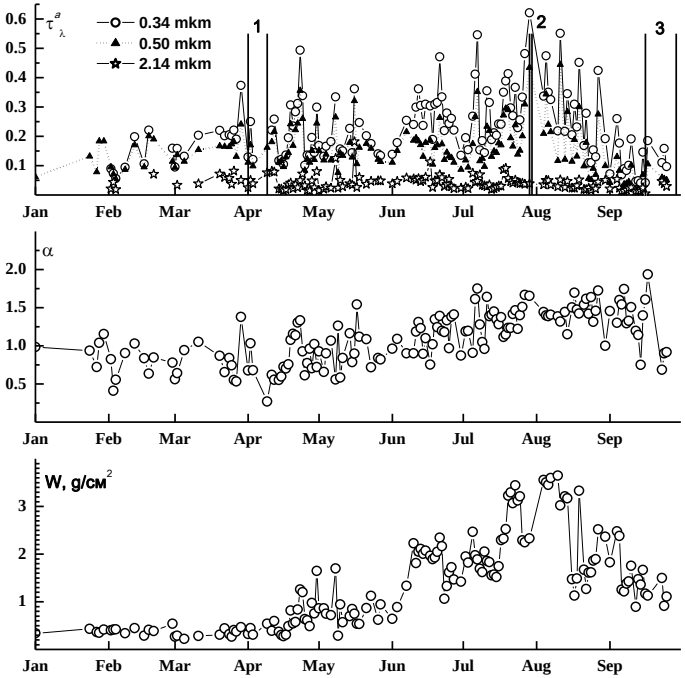

Figure 10. Time variations in the spectral AOD, Ångström exponent α, and water vapor total content W in Tomsk during 2013 (lines 1, 2, and 3 show the measurement cycles within the Experiment).

AMTD
8, 5769–5808, 2015

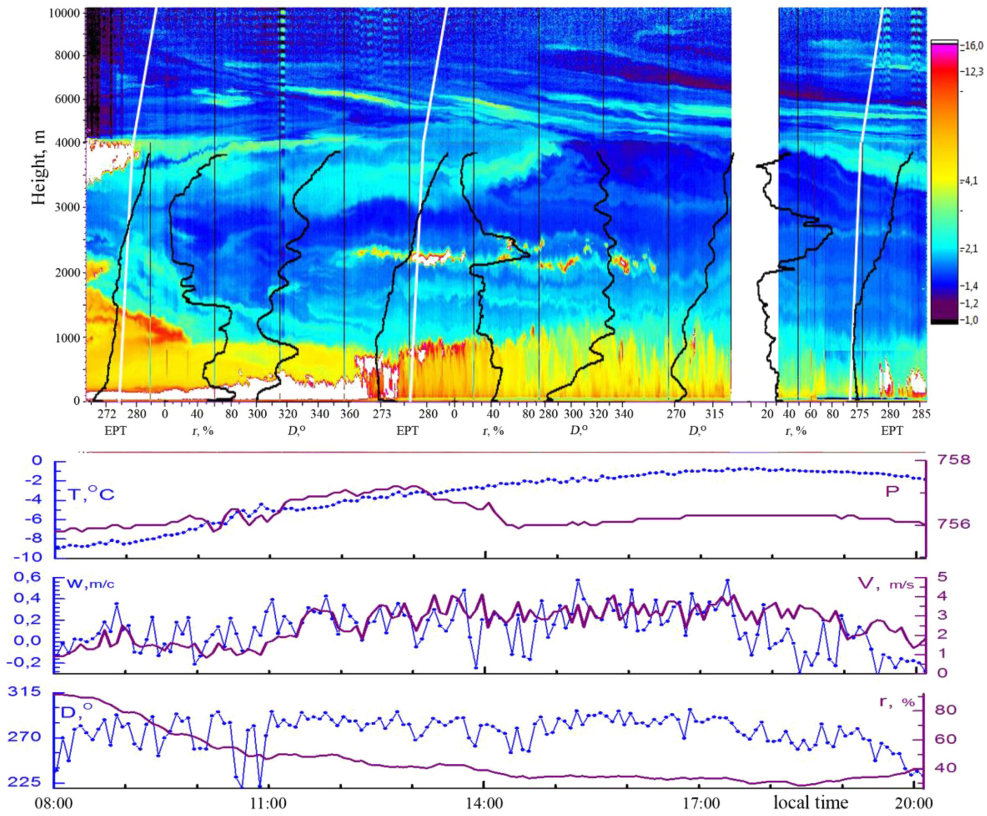

Figure 11. The aerosol structure on 3 April 2013. White lines show the ascent sonde profiles.

AMTD
8, 5769–5808, 2015

Complex experiment on stydying the microphysical propertires of aerosol particles

G. G. Matvienko et al.

CC BY

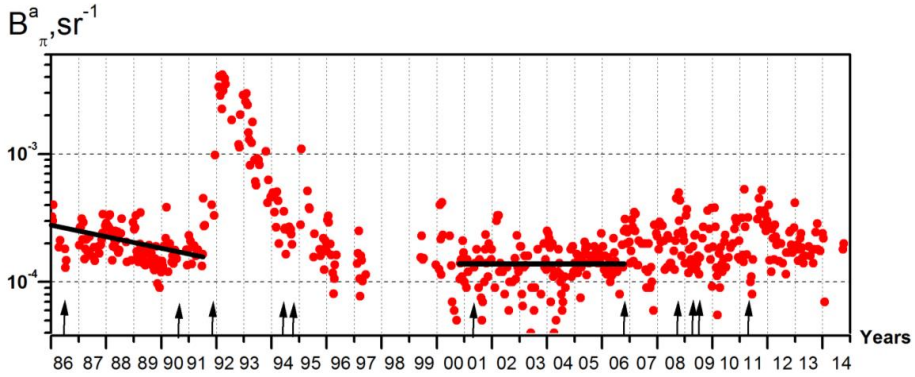

Figure 12. Time variations in the integral aerosol backscattering coefficient at a sensing wavelength of 532 nm in the altitude range 15–30 km.

AMTD
8, 5769–5808, 2015